Int. J. Electrochem. Sci., 9 **(2014)** 4394 - 4404

International Journal of
ELECTROCHEMICAL
SCIENCE
www.electrochemsci.org

Corrosion Protection of Biodegradable Magnesium Alloy Implants Using Micro-Arc Oxidation

SenWu[*], *Ya Zhang, ZhonglingWei, Yu Sheng, Xuehua zhou, Qiurong Chen*

Magnesium Alloy Technology Lab, Shanghai Institute of Microsystem and Information Technology , Chinese Academy of Science, Shanghai 200050, China.
[*]E-mail: woodwusen@gmail.com

Received: 3 April 2014 / *Accepted:* 6 May 2014 / *Published:* 19 May 2014

Magnesium alloy has good biocompatibility, biodegradation and proper mechanical properties and thereby has the potential to be used as biomedical materials. However, Magnesium alloy may corrode and degrade too quickly for application in the body. In order to improve the bioactivity and corrosion resistance of the magnesium alloy, a coating is prepared by the micro-arc oxidation (MAO) on the surface of the substrate. The performance of coated magnesium alloy is characterized using X-ray diffraction (XRD), scanning electron microscopy (SEM), energy dispersion spectrometry (EDS). The potentiodynamic polarization, electrochemical impedance spectroscopy (EIS) and immersion test are employed to evaluate the corrosion resistance and in vitro bioactivity. It is shown that an increase of corrosion resistance and improvement of the in vitro bioactivity is found on the coated magnesium alloy.

Keywords: Biodegradable magnesium alloy; coating; micro-arc oxidation; corrosion resistance

1. INTRODUCTION

Magnesium and its alloys have a number of advantages which make them an attractive choice for many applications, including aerospace component, computer parts, mobile phones, etc [1,2]. Fortunately, magnesium alloy also can be a popular candidate as an implant material due to its biodegradability, non-toxicity, and excellent mechanical and physical properties, which are similar to the properties of bones [3-5]. However, the key obstacle for their application is the fast degradation of the magnesium alloys, which needs to be addressed before surgical implantation [6]. Surface modification is widely studied in recent years in order to decrease the initial degradation rate of biodegradable magnesium alloys [7-12].

Micro-arc oxidation (MAO) is a relatively promising surface treatment method, which could generate a thick, dense and hard oxide coating, or a ceramic layer on the magnesium alloy. In the case of magnesium alloy, such coating consists mainly of MgO combined with magnesium silicates, borates, etc., depending on the chemical composition of the electrolytic bath [13,14]. However, for biomedical applications, the coating should be further enhanced. A possible solution is to design the structure of the coating components with incorporating the bioactive elements. As we know, the calcium and phosphorus are the main elements in bone tissues and Ca-P coatings have been widely used to construct new bones and promote osteointegration on biomedical implants [15,16]. Few publications have related to the preparation of the Ca-P coating with MAO technique, which needs further investigations [17-19].

In this present study, the MAO coating was prepared in the electrolyte composed of Na_3PO_4, $CaCO_3$, NaOH, and H_2O_2 and the in vitro degradation behavior of the coated alloy was analyzed using immersion and electrochemical techniques in simulated body fluid (SBF).

2. EXPERIMENTAL

2.1 Materials

The chemical compositions of the Mg alloy (Mg-3.0Nd-0.2Zn-0.4Zr, hereafter, abbreviated as JDBM) employed in this study was as follows (in wt.%): Nd 2.98%, Mn 0.1%, Zn 0.216%, Zr 0.49%, Fe 0.3%, Si 0.2%, Ni 0.1%, Cu 0.1%, and Mg balance. The samples of JDBM were cut to the size of 1.5 cm×1.5 cm×0.5 cm. Prior to anodizing, all the JDBM coupons were polished with emery paper with 600 grits. The samples were washed with distilled water in an ultrasonic bath and dried in air at room temperature. In this paper, all the solutions were prepared by using analytical grade reagents and distilled water.

2.2 Preparation of coating

For anodizing process, an AC power supply (voltage: 0~600 V; frequency: 500 Hz; duty ratio: 10%; current density: 80 mA/cm^2) was employed. The electrolyte employed to anodize the JDBM was composed of 10 g/L Na_3PO_4, 0.3 g/L $CaCO_3$, 10 g/L NaOH, and 2 g/L H_2O_2. The JDBM and the 304 stainless steel were used as the anode and cathode. After anodizing process, the samples were ultrasonically cleaned in acetone and then dried using air stream.

2.3 Evaluation of coating

The surface morphology and cross-section of the MAO coatings was examined by a scanning electron microscopy (SEM, HITACHI, S-4700). Energy dispersive spectrometry (EDS) attached to SEM was used to detect elemental composition of the MAO coatings on the magnesium alloy substrate.

The phase composition was analyzed using X-ray diffractometer (XRD, Bruker D8 ADVANCE). The film thickness was measured by a coating thickness gauge (type TT260, TIME Group Inc., Beijing, China).

Electrochemical tests were performed to study the corrosion behavior of naked-JDBM and MAO-JDBM. The simulated body fluid (SBF) [20] was used as corrosive environments at 37±1 ºC. Potentiodynamic polarization and electrochemical impedance spectroscopy (EIS) was carried out using Autolab PGSTAT 302N. Measurements were conducted in a traditional three-electrode system with the oxide coating on naked-JDBM as working electrode, a large area platinum sheet as counter electrode and a saturated calomel electrode (SCE) as reference electrode. The size of samples exposed to the electrolyte was 1 cm^2.

The immersion test was carried out in the SBF. The immersion test was carried out at different time in order to monitor the corrosion rate of naked-JDBM and MAO-JDBM. The samples was individually immersed in the SBF for a total of 60 days and the temperature of the SBF maintains at 37±1℃. The corrosion products on the surface of sample could be removed by the chromic acid. The corrosion rate of samples is calculated by the weight loss as a function of immersion time, according to equation:

$$\text{Corrosion rate} = 87.6\frac{w}{\rho A t} \qquad (1)$$

where w is the weight loss (mg), ρ is the density of the sample (g/cm^3), A is the initial area exposed to the SBF (cm^2), t is the immersion time (h).

3. RESULTS AND DISCUSSIONS

3.1 Anodized growth process

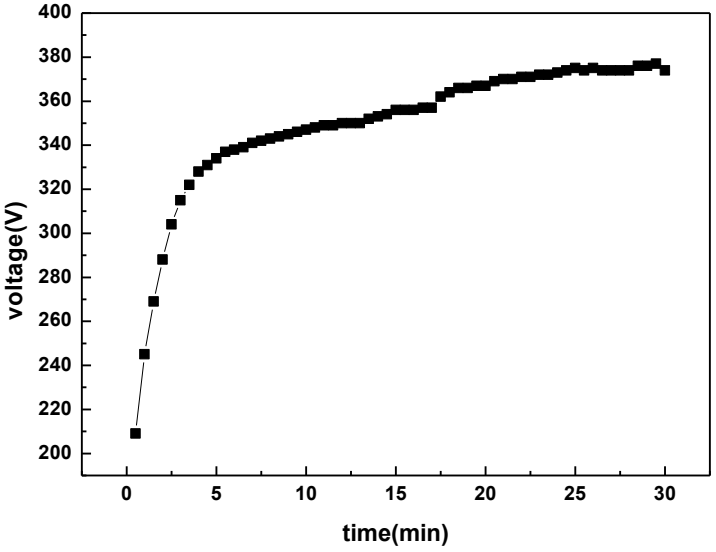

Figure 1. The potential change with time during MAO process in the electrolyte at the current density of 80 mA/cm^2

During the MAO process, the applied voltage behaved quite different with the anodizing time, as presented in figure 1. In general, the potential-time curve could be divided into three stages [21-23], stage I from 0 to 5 min, stage II from 5 to 25 min and stage III from 25 to 30 min. At the beginning of the MAO process, the potential rises almost linearly with the time and finely reach to 330 V. It is seen that several small and white sparks on the surface are appeared. With the further increasing of the cell potential, the MAO process enters into the second stage (about from 330 V to 370 V). The white sparks change into orange one and some big size of sparks can be found on the substrate surface. The MAO process becomes very fierce. During the third stage (around 370 V), the small size of sparks on the substrate surface decreases, and also the big size of sparks appears separately on the surface of specimen.

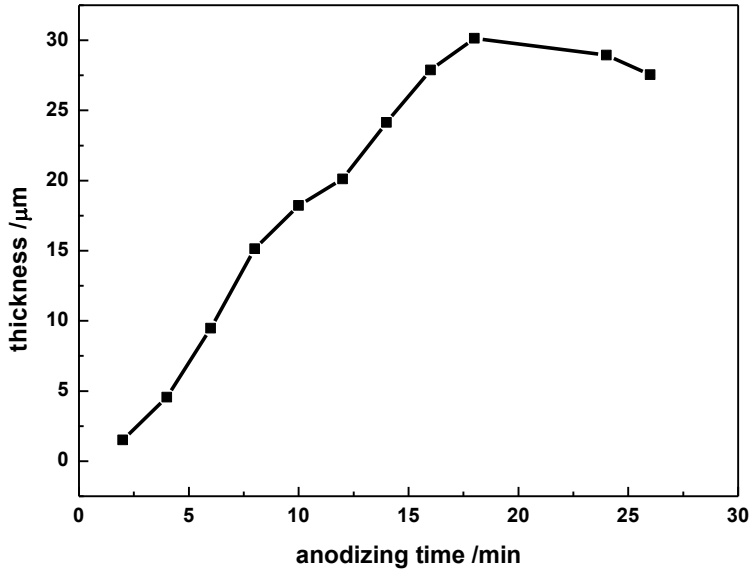

Figure 2. Effect of anodizing time on the coating thickness

To study the effect of anodizing time on the properties of MAO coatings, samples with different anodizing time are first prepared with the current density of 80 mA/cm^2. The coating thickness with different anodizing time is measured and the result is shown in figure 2. It is shown that the coating thickness goes increasingly with the anodizing time. When the anodizing time arrives to 18 min, the coating thickness gets the biggest value of 30 μm; afterwards, the coating thickness slowly decreases with further increasing of the anodizing time.

Surface and cross-sectional morphology of the anodized specimens are examined, as shown in Fig. 3. In figure 3a, the SEM image is taken when the sample is anodized for 2 min. In this situation, the potential is at the first stage, and a number of small sparks are just found on the substrate surface. As a result, the surface is covered by porous coating, but the coating was so thin and needs to further anodize. After anodizing with 14 min, the surface is wholly covered with porous coating, as shown in

figure 3b. It is depicted that a few cracks appear on the coating, which may be the result of the electric discharge with the big spark.

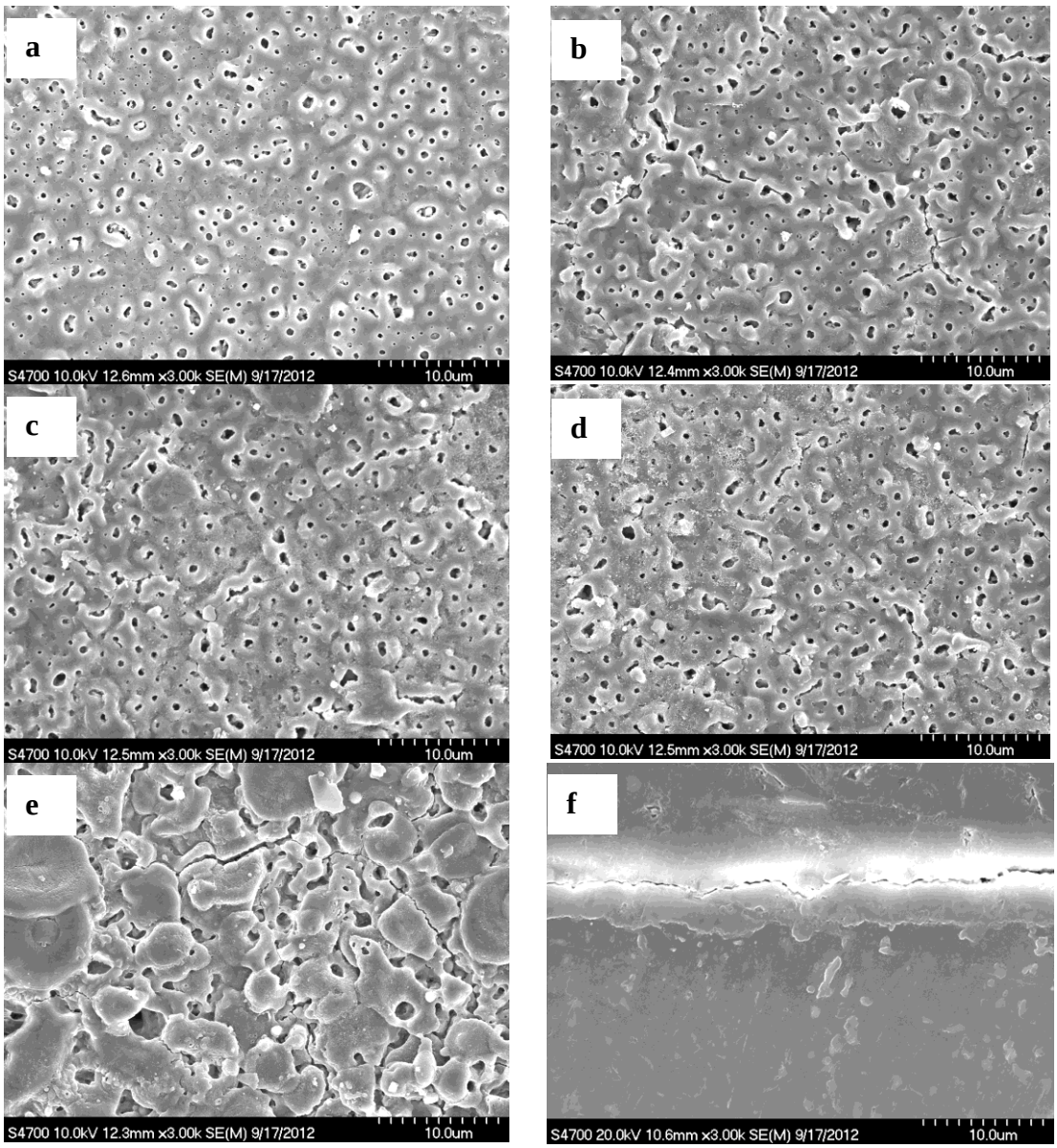

Figure 3. SEM of the surface and cross-section mophology of the specimens anodized at different time (a) 4 min, (b)14 min, (c) 16min, (d) 18 min, (e) 26 min and (f) cross-section of 18 min

The surface morphology of the specimens for 16 min and 18 min anodization has no apparent difference, as presented in figure 3c and 3d. After anodizing with 26 min, the cracks on the surface of species becomes big, duo to the big size of sparks existing in this stage. Figure 3f is the cross-sectional morphology of the specimen anodized at 18 min. It is clearly shown in figure 3f that the thickness of the coating is about 30 μm.

Figure 4 is the XRD pattern of the sample anodized with 18 min, which shows that the crystallized MgO exist in the coating. The MgO layer is formed by the dissolving Mg^{2+} outward from substrate and the oxidized oxygen O^{2-} inward from electrolyte by the reaction:

$$Mg^{2+} + O^{2-} \rightarrow MgO \quad (2)$$

However, the other compounds other than MgO could not found from the XRD pattern. This may be due to the less content of the other compounds in the MAO coating. Table 1 shows the composition of the MAO coating.

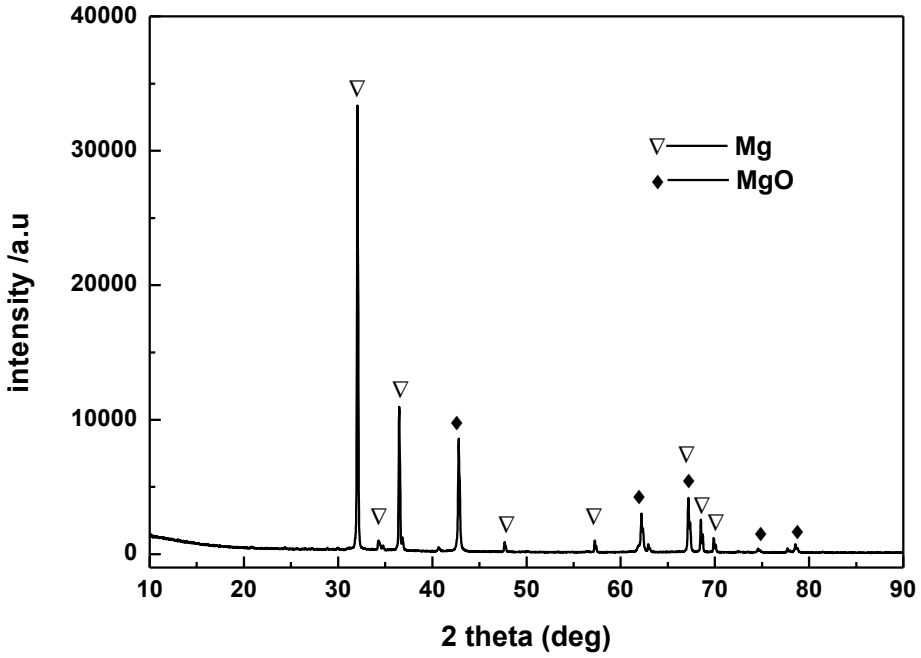

Figure 4. Typical XRD pattern of the MAO coating

Table 1. Element weight percent of MAO coating from EDS

Anodized film	Weight (%)					
	C	O	Na	Mg	P	Ca
MAO coating	38.38	11.05	0.22	43.96	4.75	1.64

It is clearly found that the MAO coating mainly composed of C, O, P, Ca and Mg as well as the trace of the Na. Based on the results of XRD and EDS, it is assumed that the MAO coating may be mainly composed of MgO, $CaCO_3$ and Ca-P compounds.

3.2 Electrochemical behavior of the MAO coatings

To evaluate the corrosion resistant properties of the JDBM with or without MAO coatings formed on the surface of the substrate, the polarization curve and EIS techniques are employed. The potentiodynamic polarization curves and electrochemical parameters are shown in figure 5 and Table 2, respectively. The corrosion potential (E_{corr}), corrosion current density (j_{corr}), and anodic/cathodic Tafel slopes (β_a and β_b) were obtained from potentiodynamic polarization curves in figure 5. These

results are summarized in Table 2. Based on the approximately linear polarization behavior near OCP (open circuit potential), the polarization resistance (R_p) values were determined by the following relationship [21].

$$R_p = \frac{\beta_a \beta_b}{2.303 j_{corr} (\beta_a + \beta_b)} \quad (3)$$

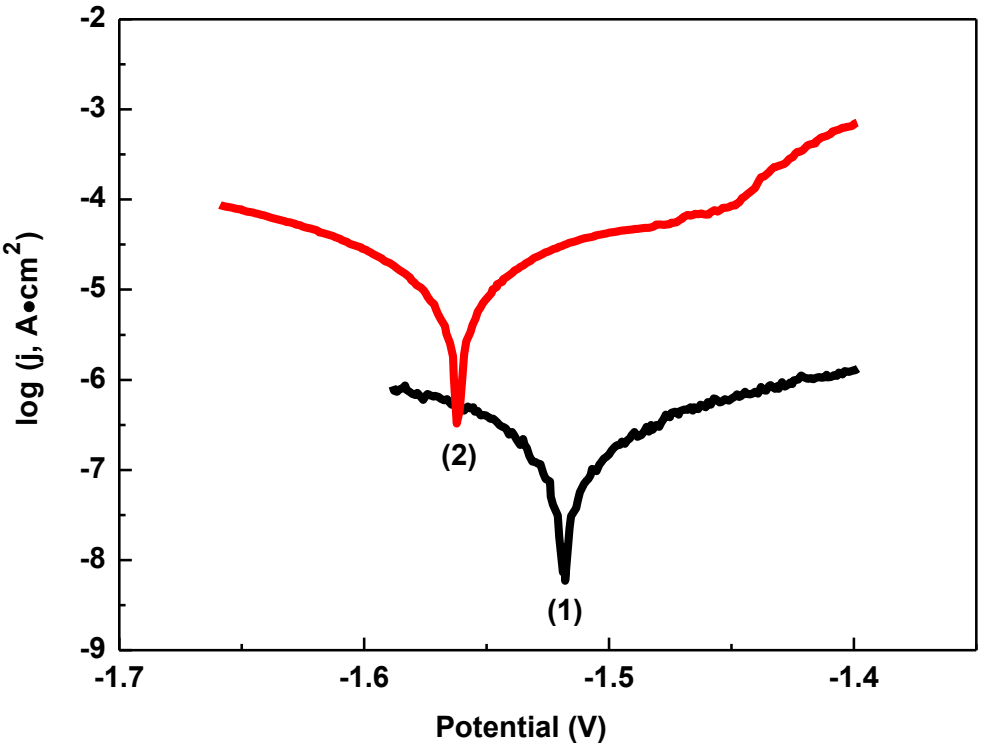

Figure 5. Potentiodynamic polarization behavior of the specimens with (1) or without (2) MAO coating on the surface of the substrate in the SBF

Table 2. Electrochemical parameters related to potentiodynamic polarization curves

	E_{corr}(V)	β_a (mV)	β_b (mV)	R_p(Ωcm^2)	j_{corr}(A/cm^2)
Naked-JDBM	-1.56	5.89	5.12	5.13×10^{4}	2.29×10^{-5}
MAO-JDBM	-1.52	6.56	4.48	2.98×10^{6}	3.89×10^{-7}

In general, good corrosion resistance can be identified by low current density, high corrosion potential, and high polarization resistance. Data and curves of figure 5 and Table 2 display clearly that j_{corr} and R_p of with the MAO coating are two orders of magnitude lower and two orders of magnitude higher than those of the uncoated magnesium alloy respectively. Meanwhile, compared to the JBDM with the -1.56 V E_{corr}, the E_{corr} of MAO coating is shifted to the positive direction, with the value of -1.52 V. In sum, the results of potentiodynamic polarization according to figure 5 and Table 2 reveal the enhancement of corrosion resistance caused by the MAO coating.

EIS diagrams of naked-JDBM substrate and the MAO-JDBM are test in the SBF at the open circuit potential, as shown in figure 6. In figure 6, the shapes and diameters of the capacitive loop

curves represent the polarization resistance of the working electrode, the higher of the polarization resistance, the stronger anti-corrosion property [22, 24-26]. The result shows the polarization resistance of naked-JDBM is 2428 Ω/m^2. The low value of the polarization resistance indicates that the naked-JDBM would be eroded easily. For the MAO-JDBM, an increase in the polarization resistance is obtained with the value of 3642 Ω/cm^2, as shown in Figure 6.

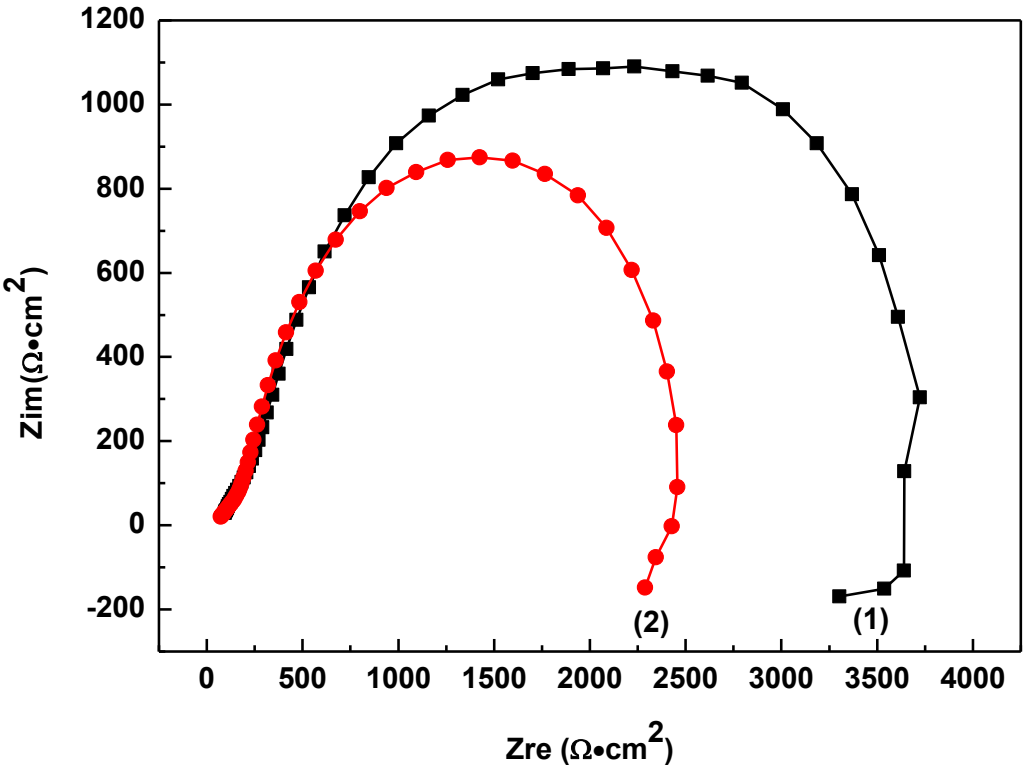

Figure 6. EIS diagrams obtained with (1) or without (2) MAO coating on the surface of the substrate in the SBF

3.3 Immersion test

To understand the in vitro corrosion resistance of naked-JDBM and MAO-JDBM with long-term degradation performance and bioactivity evaluation, the immersion test is performed. Figure 7 illustrates the SEM morphology of naked-JDBM and MAO-JDBM after 60 days immersion in the SBF. As seen from the picture (figure 7a-1), the surface of naked-JDBM was entirely covered by the corrosion product after 60 days immersion in the SBF. Also, it is found that the corrosion product is distributed with a lot of micro-holes, which led to the easily corrosion by the SBF, as shown in figure 7a-2. According to figure 7b-1, the surface of MAO-JDBM is also damaged, with many crystal products. With the further investigation, the pattern of the corrosion product is cauliflower-like structure, as presented in figure 7b-2. It is obtained that the MAO-JDBM is corroded milder than the naked-JDBM [27,28].

This specifies that the MAO coating can provide reasonable good protective layer for the substrate. We have performed the EDS examination on the surface of the naked-JDBM and MAO-JDBM after 60 days immersion in the SBF. The results are shown in Table 3. It is indicated that the elements of corrosion product of naked-JDBM are mainly composed of O, Mg, P, Ca, and C. Thus, it is obtained that the corrosion products are mainly composed of MgO, $Mg(HO)_2$, and Ca-P compound. Meanwhile, the elements of corrosion product of MAO-JDBM are mainly composed of O, Mg, Ca, and C, which indicates the crystal of $CaCO_3$, is formed on the surface of sample. This can be an indication for the decent bioactivity for the corrosion product of MAO-JDBM, and in the human body can also be absorbed by the body and metabolism.

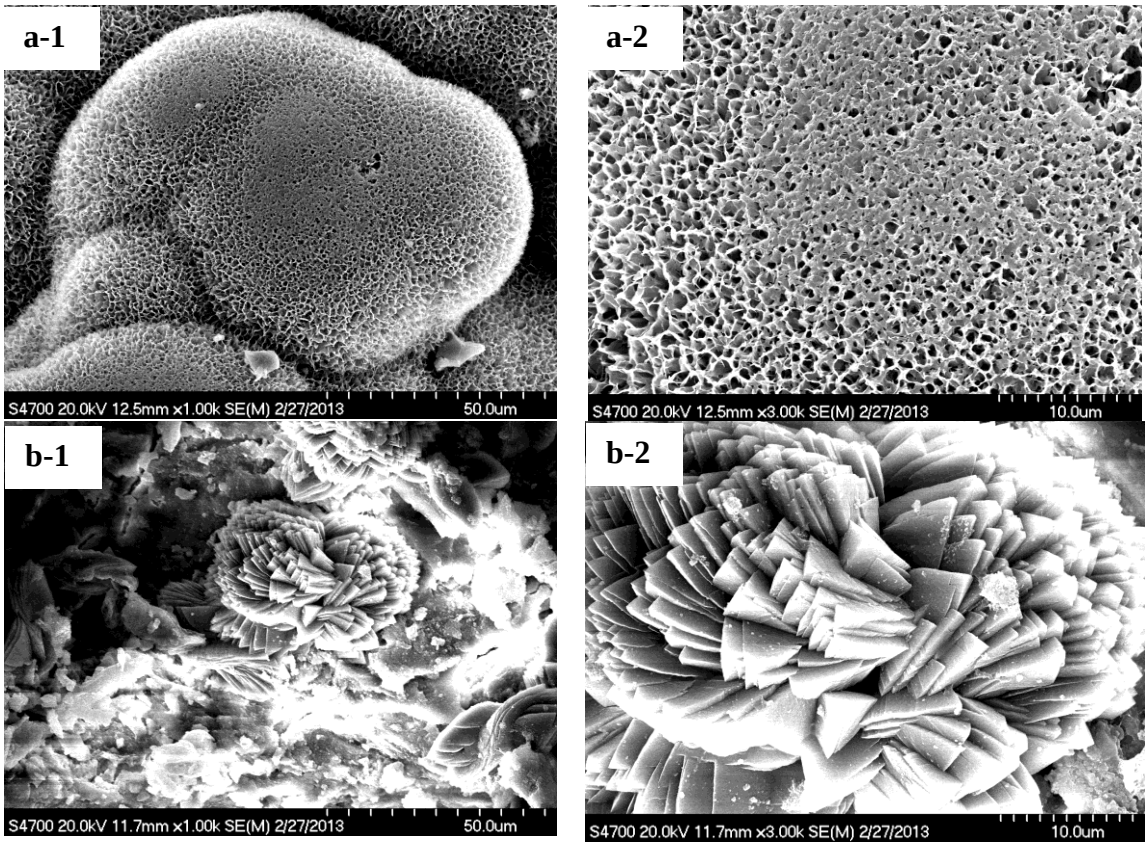

Figure 7. SEM morphology of naked-JDBM (a-1, a-2) and MAO-JDBM (b-1, b-2) samples after 60 days immersion in the SBF

As seen from the Figure 8, the corrosion rate of naked-JDBM is considerably greatly than that of the MAO-JDBM. It is obtained that the corrosion rate increased from 0.25 mm/y (measured in the first 3 days) to 0.95 mm/y (measured in 60days) with naked-JDBM and from 0.15 mm/y to 0.35 mm/y with MAO-JDBM. Therefore, the MAO-JDBM either short or long-term provides excellent corrosion resistance compared to naked-JDBM. The results of immersion tests are consistent with those of the electrochemical measurements, indicating effective protection proving by the MAO coating.

Table 3. Element weight percent of corrosion product from EDS

Anodized film	Weight (%)						
	C	O	Na	Mg	P	Cl	Ca
Naked-JDBM	14.81	60.63	0.63	21.62	0.5	0.34	1.47
MAO-JDBM	8.5	56.41	---	0.99	---	---	34.11

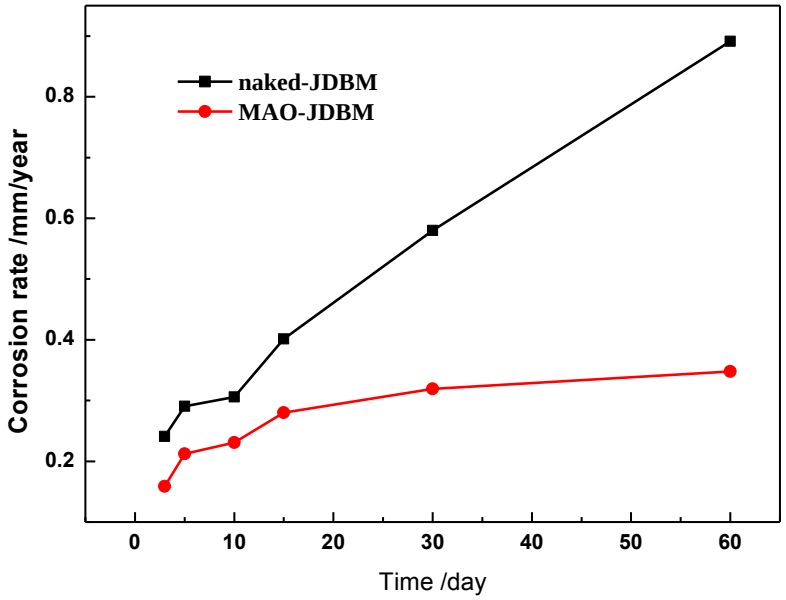

Figure 8. Corrosion rate of naked-JDBM and MAO-JDBM versus immersion time in the SBF

4. CONCLUSIONS

In this study, an oxidation coating was successfully prepared on a biodegradable magnesium alloy using the micro-arc oxidation. The best performance of MAO coating is obtained with the oxidation time 18 min. It is obtained that an increase of corrosion resistance and improvement of the in vitro bioactivity is found on the surface of MAO-JDBM compared to the naked-JDBM. And the results suggest that the surface modification of JDBM by MAO method can assist in preparing this alloy for its application as metal biodegradable bone implants. Further work should be focused on the cell compatibility and the in vivo performance of MAO coating.

ACKNOWLEDGEMENTS
This work was supported by Shanghai Scientific Research Projects (11DJ1400302).

References

1. J. E. Gray, B. Luan, *J. Alloys Compd*., 336 (2002) 88.
2. C. S. Wu, Z. Zhang, F. H. Cao, L. J. Zhang, J. Q. Zhang, C. N. Cao, *Appl. Surf. Sci*., 253 (2007)

3893.
3. F. Witte, V. Kaese, H. Haferkamp, E. Switze, *Biomaterials*, 26 (2005) 3557.
4. M. P. Staiger, A. M. Pietak, J. Huadmai, G. Dias, *Biomaterials*, 27 (2006) 1728.
5. F. Witte, J. Fischer, J. Nellesen, H. Crostack, V. Kaese, A. Pischd, F. Beckmann, H. Windhagen, *Biomaterials*, 27 (2006) 1013.
6. J. E. Gray, B. Luan, *J. Alloys Compd*., 336 (2002) 88.
7. L. Li, J. Gao, Y. Wang, *Surf. Coat. Technol*. 185 (2004) 92.
8. J. D. Majumdar, U. Bhattacharyya, A. Biswas, I. Manna, *Surf. Coat. Technol*., 202 (2008) 3638.
9. Y. Z. Wan, G. Y. Xiong, H. L. Luo, F. He, Y. Huang, Y.L. Wang, *Appl. Surf. Sci*., 254 (2008) 5514.
10. A. C. Hänzi, P. Gunde, M. Schinhammer, P. J. Uggowitzer, *Acta Biomater*., 5 (2009) 162.
11. M. Jönsson, D. Persson, D. Thierry, *Corros. Sci*., 49 (2007) 1540.
12. Y. Xin, K. Huo, H. Tao, G. Tang, P. K. Chu, *Acta Biomater*., 4 (2008) 2008.
13. J. H. Gao, S. K. Guan, J. Chen, L. G. Wang, S. J. Zhu, J. H. Hu, Z. W. Ren, *Appl. Surf. Sci*., 257 (2011) 2231.
14. Z. Yao, L. Li, Z.Jiang, *Appl. Surf. Sci*., 255 (2009) 6724.
15. S. V. Dorozhkin, *J. Mater. Sci*., 42 (2007) 1061.
16. S. Shadanbaz, G. J. Dias, *Acta Biomater*., 8 (2012) 20.
17. D. Sreekanth, N. Rameshbabu, *Mater. Lett*., 68 (2012) 439.
18. A. Seyfoori, S. Mirdamadi, Z. S. Seyedraoufi, A. Khavandi, M. Aliofkhazraei, *Mater. Chem. Phys*., 142 (2013)87.
19. X. Lin, L. Tan, Q. Zhang, K. Yang, Z. Hu, J. Qiu, Y. Cai, *Acta Biomater*., 9 (2013) 8631.
20. T. Kokubo, H. Takadama, *Biomaterials*, 27 (2006) 2907.
21. D. Y. Hwang, Y. M. Kim, D. –Y. Park, B. Yoo, D. H. Shin, *Electrochim. Acta*, 54 (2009) 5479.
22. D. Veys-Renaux, E. Rocca, G. Henrion, *Electrochem. Commun*., 31 (2013) 42.
23. A. Bai, Z. –J. Chen, *Surf. Coat. Technol*., 203 (2009) 1956
24. X. Guo, M. An, P. Yang, H. Li, C. Su, *J. Alloys Compd*. 482 (2009) 487.
25. Y. Liu, Z. Wei, F. Yang, Z. Zhang, *J. Alloys Compd*. 509 (2011) 6440.
26. H.-Y Hsiao, H.-C. Tsung, W.-T Tsai, *Surf. Coat. Technol*. 199 (2005) 127.
27. S. V. Dorozhkin, *Acta Biomater* (2014), http://dx.doi.org/10.1016/j.actbio.2014.02.026
28. Y. K. Pan, C. Z. Chen, D. G. Wang, Z. Q. Lin, *Mater. Chem. Phys*. 141 (2013) 842.